Hindawi
International Journal of Energy Research
Volume 2024, Article ID 2120442, 10 pages
https://doi.org/10.1155/2024/2120442

Research Article

Enhancing Strategy of Triboelectric Nanogenerator via Origami Pattern by Harvesting Mechanical Motion and Wind Flow

Seh-Hoon Chung,[1] Minsoo Kim,[1] Zong-Hong Lin,[2] Bonwook Koo,[3] Dongwhi Choi,[4] Dongseob Kim,[5] and Sangmin Lee[1]

[1]*School of Mechanical Engineering, Chung-ang University, 84, Heukseok-ro, Dongjak-gu, Seoul 06974, Republic of Korea*
[2]*Department of Biomedical Engineering, National Taiwan University, Taipei 10167, Taiwan*
[3]*Major in Wood Science and Technology, Kyungpook National University, 80 Daehakro, Daegu 41566, Republic of Korea*
[4]*Department of Mechanical Engineering (Integrated Engineering Program), Kyung Hee University, Yongin, Gyeonggi 17104, Republic of Korea*
[5]*Safety System R&D Group, Korea Institute of Industrial Technology (KITECH), 57, Yangho-gil, Yeongcheon-si, Gyeongsangbuk-do 38822, Republic of Korea*

Correspondence should be addressed to Dongwhi Choi; dongwhi.choi@khu.ac.kr, Dongseob Kim; yusae@kitech.re.kr, and Sangmin Lee; slee98@cau.ac.kr

Received 15 November 2023; Revised 3 January 2024; Accepted 18 April 2024; Published 15 May 2024

Academic Editor: Geng Chen

Triboelectric nanogenerators (TENGs) are promising energy-harvesting devices that generate electricity from mechanical energy. However, the electrical outputs of typical TENGs are limited because of the fundamental mechanism by which TENGs require a certain amount of space for contact-separation motion. Therefore, we developed an origami-based vertical/fluttering hybrid TENG (OVFH-TENG), which is the innovative structure that can generate electricity from both vertical movement and wind flow which is generated by vertical movement. It consists of a vertical TENG and a fluttering TENG where vertical TENGs can generate electricity and wind flow from mechanical input and the fluttering TENGs can generate electricity from the wind flow which is generated by its own operation process. Thus, OVFH-TENG can effectively harvest energy from vertical contact and fluttering motions with a single input. The optimized OVFH-TENG generated a 34.7% higher output than the general contact-separation TENG. Finally, the OVFH-TENG was able to light 180 LEDs, which was not possible with a general contact-separation TENG.

1. Introduction

Triboelectric nanogenerators (TENGs) are promising energy-harvesting devices that convert mechanical input into electrical output through the combined effect of electrostatic induction and triboelectrification [1–5]. TENGs have unique advantages in terms of materials and design, including low weight, low cost, and high applicability, making them the preferred devices for portable electronics and self-powered sensors [6–9]. Despite their various advantages, TENGs have limitations because they generate only low electrical power for real-life applications. To overcome this limitation, several studies have been conducted to enhance the electrical output of TENGs, such as increasing the surface charge density by suppressing the air breakdown effect [10–12], increasing the contact surface with a mechanical structure [13–15], and utilizing additional circuits, such as charge excitation circuits [16–18]. However, although several strategies for enhancing the electrical output of TENGs have been reported, TENGs still have limited electrical output owing to the space constraints of the fundamental mechanism. Several researchers have reported TENG structures that can reduce space constraints, such as multilayer or stacked TENGs; however, these structures can only be utilized under certain conditions, such as sliding- or rotating-type TENGs [19, 20]. Therefore, various strategies are needed to maximize the electrical output of

TENGs within a given structure size to enable their utilization under a variety of conditions for the improvement of TENG.

In this study, we introduce an origami-based vertical/fluttering hybrid TENG (OVFH-TENG), which is a hybrid generator consisting of a vertical TENG and a fluttering TENG. OVFH-TENG is first introduced strategy that can generate electricity from additional wind which is generated with its own operation by designing fluttering TENG under the OVFH-TENG. Using the Yoshimura origami pattern [21], which consists of isosceles triangles and repeated rhombus shapes, the OVFH-TENG was structured as a 3-D cylindrical structure using a piece of film. Depending on the structural characteristics of the Yoshimura pattern, which is flat when pressed vertically and returns to its original state when removed, it can be used as a vertical TENG, which is a typical TENG that produces an output according to the contact-separation motion. Moreover, wind flow is generated by pressing and releasing the structure, owing to the empty space inside the Yoshimura-patterned cylinder. Therefore, the OVFH-TENG includes a fluttering TENG at the bottom to generate additional electricity from the wind flow. Because the vertical and fluttering TENGs are operated with the same input energy, they can exhibit synergy as a hybrid generator that produces a high output compared to its limited size. In addition, to optimize the structure of the OVFH-TENG for an enhanced electrical output, we analyzed the surface contact area and internal volume of the OVFH-TENG using mathematical and experimental data. Consequently, the optimized OVFH-TENG produced 34.7% higher output than a general TENG. Accordingly, the electrical output of the OVFH-TENG was enhanced compared with that of a general TENG with the same input energy and operating space.

2. Materials and Methods

2.1. Fabrication of OVFH-TENGs. The OVFH-TENG consisted of a polyimide sheet, polymethylmethacrylate (PMMA) plate (diameter: 13 cm and thickness: 0.2 cm), pillar (length: 4 cm, width: 0.2 cm, and height: 1 cm), and aluminum tape (thickness: 0.05 mm (Ducksung Hitech Co.)). A polyimide (PI) film was used as the main body of the vertical TENG structure and as the fluttering film of the fluttering TENG. The frames of the vertical TENG and fluttering TENG are composed of PMMA. The PMMA pillars were used to provide a path and space for the wind to flow through the fluttering TENG. The aluminum tape was attached to the bottom PMMA plate between the PMMA pillars, and the folding part of the vertical TENG was connected to an electric wire. In addition, ultrafast switching diodes (MUR460, Motorola Co.) were used in the rectification circuit of the OVFH-TENG. Commercial green LEDs (5BG4UC00, Dakwang Co.) were used to evaluate the application.

2.2. Electrical Measurements. The voltage outputs were measured using an oscilloscope (MDO 3014, Tektronix Co.), and the current outputs were measured using an electrometer (model 6514, Keithley).

3. Result and Discussion

Figure 1(a) shows a schematic of the OVFH-TENG, which consists of a vertical TENG that can generate electricity by contact-separation movement and a fluttering TENG that can generate electricity by wind input. A photograph of the OVFH-TENG is shown in Figure S1. The vertical TENG was structured using a PI film and attaching the electrode on the PI film between two acrylic substrates. As PI is a well-known negatively charged material, the vertical TENG can generate electricity from the negative surface charge of the PI film. The fluttering TENG was located under the vertical TENG. The fluttering TENG comprises three symmetrical sections: an acrylic substrate, an aluminum electrode on the bottom substrate, and a PI film. In addition, there was a hole at the center of the upper substrate of the fluttering TENG and the bottom substrate of the vertical TENG; thus, the wind flow from the vertical TENG could be transferred to the fluttering TENG. A schematic of the wind flow inside the vertical TENG and fluttering TENG is shown in Figure S2. Therefore, when the OVFH-TENG was pressed from the top, the vertical TENG folded, and the air inside the vertical TENG flowed into the fluttering TENG. Thus, the PI film of the fluttering TENG was fluttered by the wind input. As a result, both the vertical and fluttering TENG can be operated by a pressing movement.

A schematic of the working mechanism of the vertical TENG is shown in Figure 1(b). The vertical TENG operates in single-electrode mode, which generates an electric output by contact separation between the PI film and the single electrode attached to the bottom isosceles surface. When the upper isosceles PI film surface contacts the electrode, free electrons flow from the single electrode to the electrical ground owing to the negative surface charge of the PI film. When the upper PI film surface is separated from the lower electrode, electrons flow in the opposite direction from the electrical ground to the single electrode, causing an electric current. Consequently, vertical TENG can generate electricity through a pressing movement.

Figure 1(c) shows the working mechanism of the fluttering TENG. The fluttering TENG was operated by the contact-separation motion between the PI film in the fluttering TENG and the electrode on the bottom acrylic substrate. When the PI film was fluttered by the wind flow, a part of the PI film contacted and separated from the bottom electrode. When the PI film was in contact with the electrode, the electrons inside the bottom electrode were transferred to the ground. When the PI film separated from the electrode, electrons were transferred from the ground to the electrode. Using this electron flow, the fluttering TENG can also generate electrical output from the wind flow caused by the pressing movement.

To optimize the design of the OVFH-TENG, a mathematical study of the design of the planar origami pattern is necessary. Figure 2 shows the definitions of the design parameters of the OVFH-TENG and the optimization of the 3-D origami structure through mathematical studies. As the OVFH-TENG can generate electric output by the vertical and fluttering TENG, the structure of the OVFH-TENG

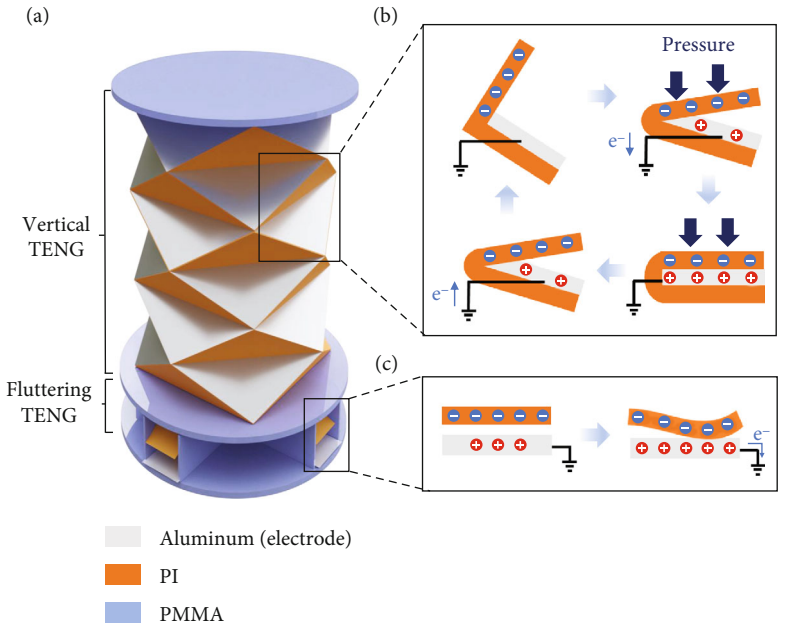

Figure 1: Origami-based vertical/fluttering hybrid triboelectric nanogenerator (OVFH-TENG): (a) schematic of the structure of OVFH-TENG. Schematic of the working mechanism of (b) vertical TENG and (c) fluttering TENG.

was optimized by maximizing the surface and volume areas of the 3-D origami structure to increase the surface area of the vertical TENG and the wind flux to the fluttering TENG. Therefore, mathematical studies using the design parameters were conducted to determine the maximum volume and surface area of the 3-D origami structure. The 2-D planar figure of the origami pattern is composed of isosceles triangles and repeated rhombus shapes. The design parameters of the origami pattern are shown in Figure 2(a), as mentioned by Suh et al. in 2021 [22]. m is the number of isosceles triangles in width, n is the number of rows in height, θ is the apex angle of the isosceles triangle, and a is the leg length of the isosceles triangle. In this study, m, n, and a were set to 4, 6, and 5 cm, respectively.

A schematic of the origami structure is shown in Figures 2(b) and 2(c). The volume of the 3-D origami structure V is calculated as follows:

$$V = n\pi r^2 h, \tag{1}$$

where r is the radius of the structure from the top view and h is the height of the single stage of the structure. In addition, based on the relationship between the design parameters and Pythagorean theorem, h can be expressed as follows:

$$h = a\cos\frac{\theta}{2}\sqrt{1-\tan^2\frac{\theta}{2}\left\{\frac{\cos\varnothing}{(1+\sin\varnothing)}\right\}^2}, \tag{2}$$

where $\varnothing$ is the half of the interior angle of a regular polygon, and it can be obtained as follows:

$$\varnothing = \frac{\pi(m-4)}{2m}. \tag{3}$$

By combining equations (2) and (3), h can be expressed as follows:

$$h = a\cos\frac{\theta}{2}\sqrt{1-\tan 2\frac{\theta}{2}\left\{\frac{\cos(\pi(m-4)/2m)}{(1+\sin(\pi(m-4)/2m))}\right\}^2}. \tag{4}$$

r can be expressed as follows:

$$r = a\sin\frac{\theta}{2}\sec\frac{\pi(m-4)}{2m}. \tag{5}$$

Therefore, by combining equations (1), (4), and (5), V can be described as follows:

$$V = n\pi a^3\sin^2\frac{\theta}{2}\cos\frac{\theta}{2}\sec^2\frac{\pi(m-4)}{2m}\cdot\sqrt{1-\tan 2\frac{\theta}{2}\left\{\frac{\cos(\pi(m-4)/2m)}{(1+\sin(\pi(m-4)/2m))}\right\}^2}. \tag{6}$$

In addition, A, which is the total surface area of the structure excluding the noncontact area when pressed, can be defined as follows:

$$A = \frac{m(n-1)a^2}{2}\sin\theta. \tag{7}$$

Therefore, because m, n, and a are constants in this study, the volume and total area of the origami structure can be calculated as θ using equations (6) and (7).

Figure 2(d) shows the change in volume V according to the change in apex angle θ. As shown in the graph, V increases in the interval where θ decreases from 2.356 rad

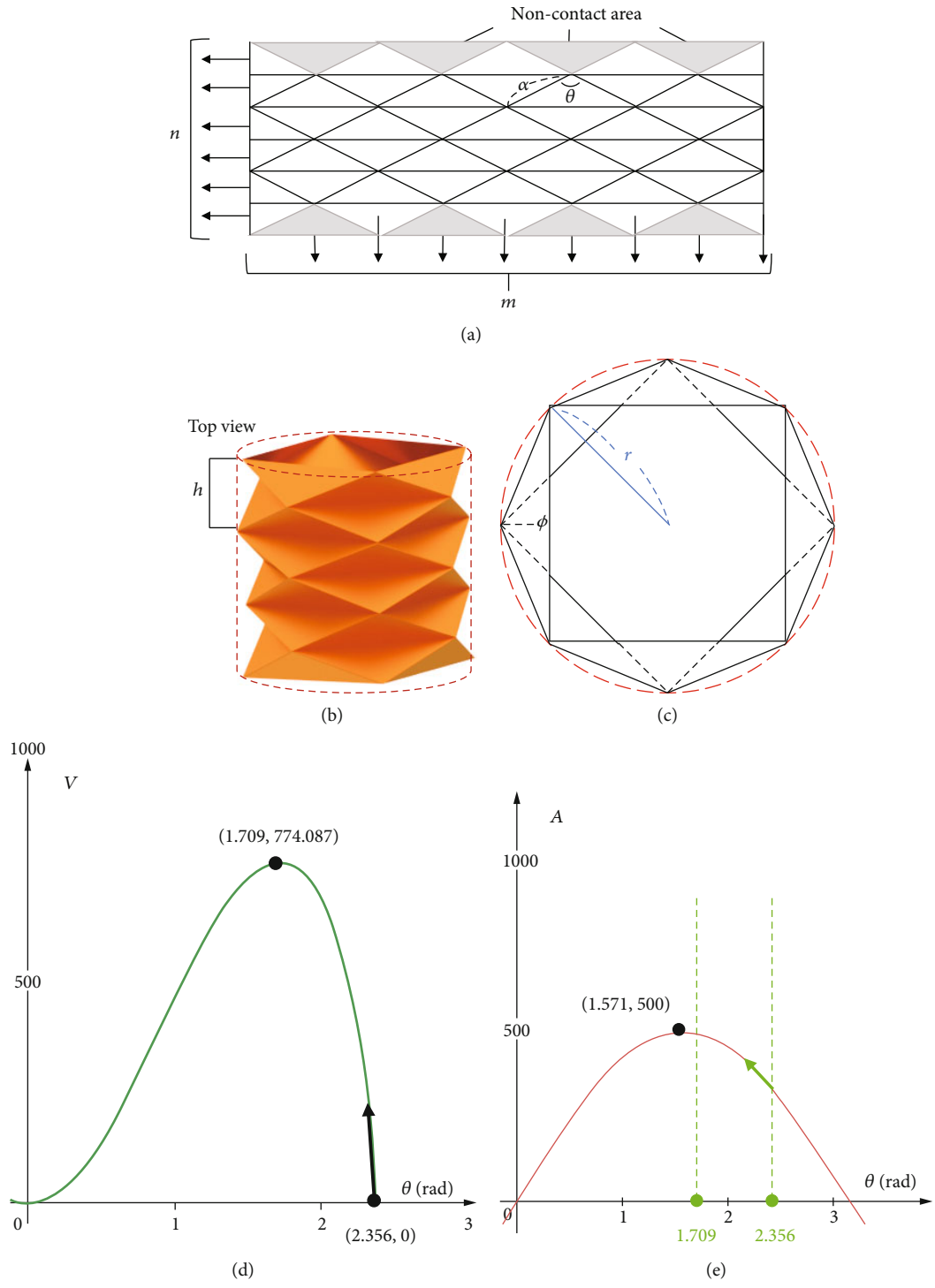

Figure 2: Optimization of origami pattern for OVFH-TENG: (a) 2-D planar figure of the origami pattern. Schematic of vertical TENG in (b) 3-D and (c) top view. (d) Calculated V graph with different θ. (e) Calculated A graph with different θ.

to 1.709 rad. As shown in Figure 2(e), the section in which the surface area A is increased includes a section in which V is increased from 3.142 to 1.571 rad. Accordingly, θ with maximized volume and surface area can be considered to be 1.709 rad. However, the pressing experiment has confirmed that when θ is below 2.214 rad, it does not fold smoothly, as shown in Figure S3. Considering both experimental and mathematical studies, the optimal structure was derived when θ was 2.214 rad.

Several studies were conducted to determine the optimum thickness of the PI film for the vertical TENG, as shown in Figure 3. Figure 3(a) shows a schematic diagram of a single-stage vertical TENG. Even with different PI film thicknesses, the vertical TENG maintained its pattern. However, if

the thickness is too thin, the initial height is low owing to the low elasticity of the thin film (Figure 3(b)), and if the thickness is too high, the attached electrode partially contacts the PI film, resulting in a low output (Figure 3(c)). Consequently, different voltage outputs were measured for different film thicknesses, which is shown in Figure 3(d). The root mean square (RMS) values of the voltage output and the average peak voltage are shown in Figure 3(e). The RMS value was calculated using the following equation:

$$\text{RMS voltage} = \sqrt{\frac{1}{T}\int V(t)^2 dt}, \tag{8}$$

where $V(t)$ is the measured voltage output over time and T is the total time. According to the results, the vertical TENG generated the highest peak and RMS voltage output with a 0.08 mm thickness of PI film. To measure the electrical output for vertical TENG, the mechanical input was given with manually in 4 Hz of input frequency.

In addition, the number of attached electrodes in the vertical TENG resulted in different outputs owing to the large contact area. Figure S4 shows the electrical output when 1, 3, 5, 7, and 9 electrodes are attached to a vertical TENG. The electrical output of the vertical TENG increases when more electrodes are attached, and the vertical TENG generates the highest voltage output when nine electrodes are attached. This result indicates that the vertical TENG can generate a high electrical output when more electrodes are attached to the PI film.

Moreover, to optimize the structure of the fluttering TENG for an enhanced output, its electrical output of fluttering TENG was measured by considering various factors. A schematic of the fluttering TENG with the design factors is shown in Figure 4(a). As shown in Figures 4(b)–4(e), the film material, film length ratio, film width ratio, and film thickness were considered to optimize the electrical output of the fluttering TENG. The measured outputs of fluttering TENGs in Figure 4 are tested with attaching vertical TENG on the top, and the 4 Hz of mechanical input was given manually to the vertical TENG.

Figure 4(b) shows the RMS voltage and average peak voltage of the fluttering TENG with the paper, PP, PI, nylon, and PTFE films. The RMS voltages of the fluttering TENG with paper, PP, PI, nylon, and PTFE films were 1.03, 3.99, 8.13, 5.61, and 1.28 V, respectively. The average peak voltages of the fluttering TENG with paper, PP, PI, nylon, and PTFE films are 2, 22.9, 43.4, 36.4, and 3.3 V, respectively. According to the result, the fluttering TENG generated the highest RMS voltage and average peak voltage when the PI film was used for the fluttering film. Although PTFE generally has a higher surface charge density than PI, a fluttering TENG can generate a higher electrical output with a PI film owing to the mechanical properties of the PI film [23, 24]. Therefore, the PI film was selected for fabricating the fluttering TENG.

Figure 4(c) shows RMS voltage and average peak voltage of fluttering TENG with different film length ratio. The film length ratio is calculated as follows:

$$\begin{aligned}\text{Film length ratio} &= \frac{I}{L},\\ \text{Film width ratio} &= \frac{w}{W},\end{aligned} \tag{9}$$

where L is the pillar length and I is the film length. The RMS voltages of fluttering TENG with film length ratios of 0.5, 0.75, 0.9, 0.95, 1, 1.25, 1.5, and 1.8 are measured as 1.86, 3.44, 5.69, 7.21, 5.84, 5.5, 3.58, and 1.51 V, respectively. The average peak voltages with film length ratios of 0.6, 0.8, 1.0, 1.2, 1.4, 1.6, and 1.8 are measured as 10.5, 23.4, 32.9, 43.1, 36.1, 33.1, 27.3, and 9 V, respectively. Because the fluttering TENG can generate electricity by the contact-separation motion between the fluttering film and the attached electrode, the electrical output can be decreased by a film length ratio of less than 1. Moreover, if the film length ratio is higher than 1, which indicates that the film is longer than the pillar, the fluttering TENG can generate a lower output owing to the unstable fluttering motion. Accordingly, the highest output was generated by fabricating a fluttering film with a film-length ratio of 0.95.

The RMS voltage and average peak voltages of the fluttering TENG with different film width ratios are shown in Figure 4(d). The film width ratio was calculated as follows:

$$\text{Film width ratio} = \frac{w}{W}, \tag{10}$$

where w is the film width and W is the width between the pillars. The RMS voltages of fluttering TENG with film width ratios of 0.4, 0.5, 0.6, 0.7, 0.8, 0.9, and 0.95 of film width ratio are measured as 2.81, 3.10, 4.53, 5.28, 7.03, 8.23, and 3.78 V, respectively, and the average peak voltages of fluttering TENG with film width ratios of 0.4, 0.5, 0.6, 0.7, 0.8, 0.9, and 0.95 of film width ratio are measured as 5.95, 9.42, 17.67, 22.58, 32.33, 44.91, and 11.34 V, respectively. The electrical output gradually increased with the film width ratio; however, the voltage output decreased when the film width ratio was 0.95. When the film width ratio was 0.95, the film width was most similar to the width between the pillars; therefore, the film contacted the pillars during fluttering. Consequently, the electrical output of the fluttering TENG decreased when the film width ratio was 0.95. Accordingly, the fluttering TENG generated the highest output with a film width ratio of 0.9.

In addition, the electrical outputs of the fluttering TENG with different film thicknesses were measured, as shown in Figure 4(e). The measured RMS voltages were 3.28, 7.81, 3.16, 2.78, and 2.12 V for film thicknesses of 0.025, 0.05, 0.075, 0.1, and 0.13 mm, respectively. In addition, the average peak voltages were 20.99, 41.13, 21.54, 18.17, and 6.375 V for film thicknesses of 0.025, 0.05, 0.075, 0.1, and 0.13 mm, respectively. Consequently, the fluttering TENG generated the highest output with a film thickness of 0.05 mm. With a thinner film thickness of 0.025 mm, the fluttering film exhibited an unstable fluttering motion; therefore, a low voltage could be generated. In addition, a thicker film can generate a lower output because of the fluttering

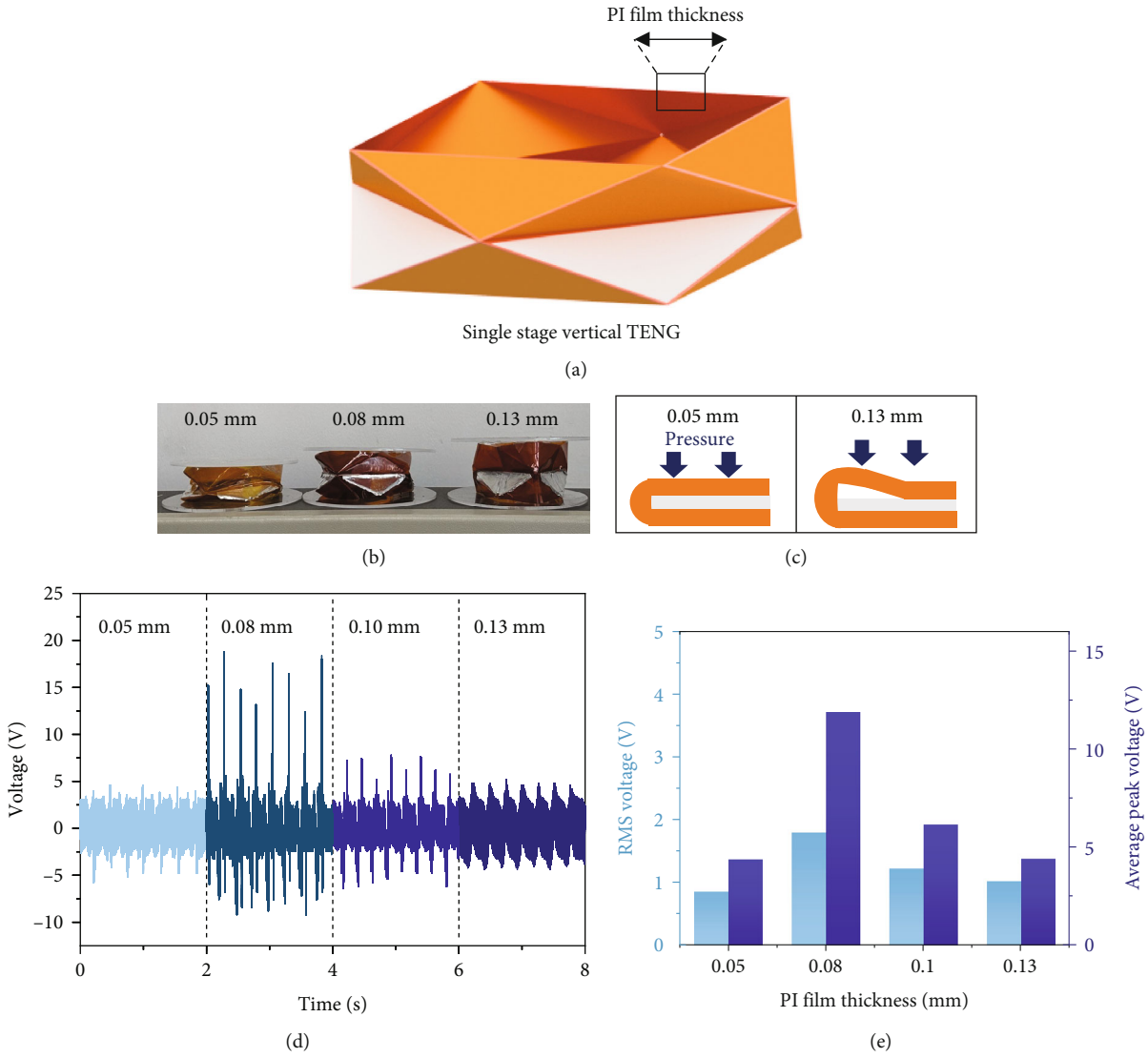

Figure 3: Optimization of PI film thickness of vertical TENG: (a) schematic of single stage vertical TENG; (b) photograph that shows the initial height with different PI film thickness; (c) schematic of vertical TENG when pressure is given; (d) voltage graph of vertical TENG with different film thickness; (e) calculated RMS voltage and average peak voltage of vertical TENG with different film thickness.

motion caused by the weight and flexibility of the film. Therefore, the highest electrical output is generated at a film thickness of 0.05 mm.

Additionally, as the wind speed can affect the electrical output performance of fluttering TENG, wind speeds that generated from vertical TENG with different input frequencies have been measured as Figure S5. As shown in the graph, the wind speed increased when the input frequency increases. 1.23, 1.78, 2.95, 4.01, and 5.91 m/s of wind speed are measured with input frequencies of 1, 2, 3, 4, and 5 Hz, respectively. Also, the voltage outputs of fluttering TENG with different vertical input frequencies are measured in Figure S6. As shown in the graph, both peak voltage and output frequency increased as the vertical input frequency increased. Therefore, this result indicates that the fluttering TENG can generate higher output with the higher wind speed and vertical TENG can generate higher wind speed with higher input frequency.

Moreover, to consider the durability of vertical TENG and fluttering TENG, the voltage outputs of vertical TENG and fluttering TENG before and after 80,000 cycles are measured in Figure S7-8. As it is unable to test durability with manual input, the vertical TENG was tested by using vibration tester and the fluttering TENG was tested by using wind blower. The input frequency was 20 Hz to test the vertical TENG, and 12 m/s of wind was used for testing fluttering TENG. As shown in Figure S7-8, both voltage outputs of vertical TENG and fluttering TENG are maintained the output voltage after 80,000 cycles. This result indicates that the OVFH-TENG can be used for long duration time.

To utilize the electrical outputs from both the vertical and fluttering TENG, a rectifying circuit is necessary for the OVFH-TENG. The OVFH-TENG and electrical circuit are shown in Figure 5(a). Figure 5(b) shows the integrated voltage outputs of the vertical and fluttering TENG. In addition, Figure 5(c) shows the current output of the fluttering

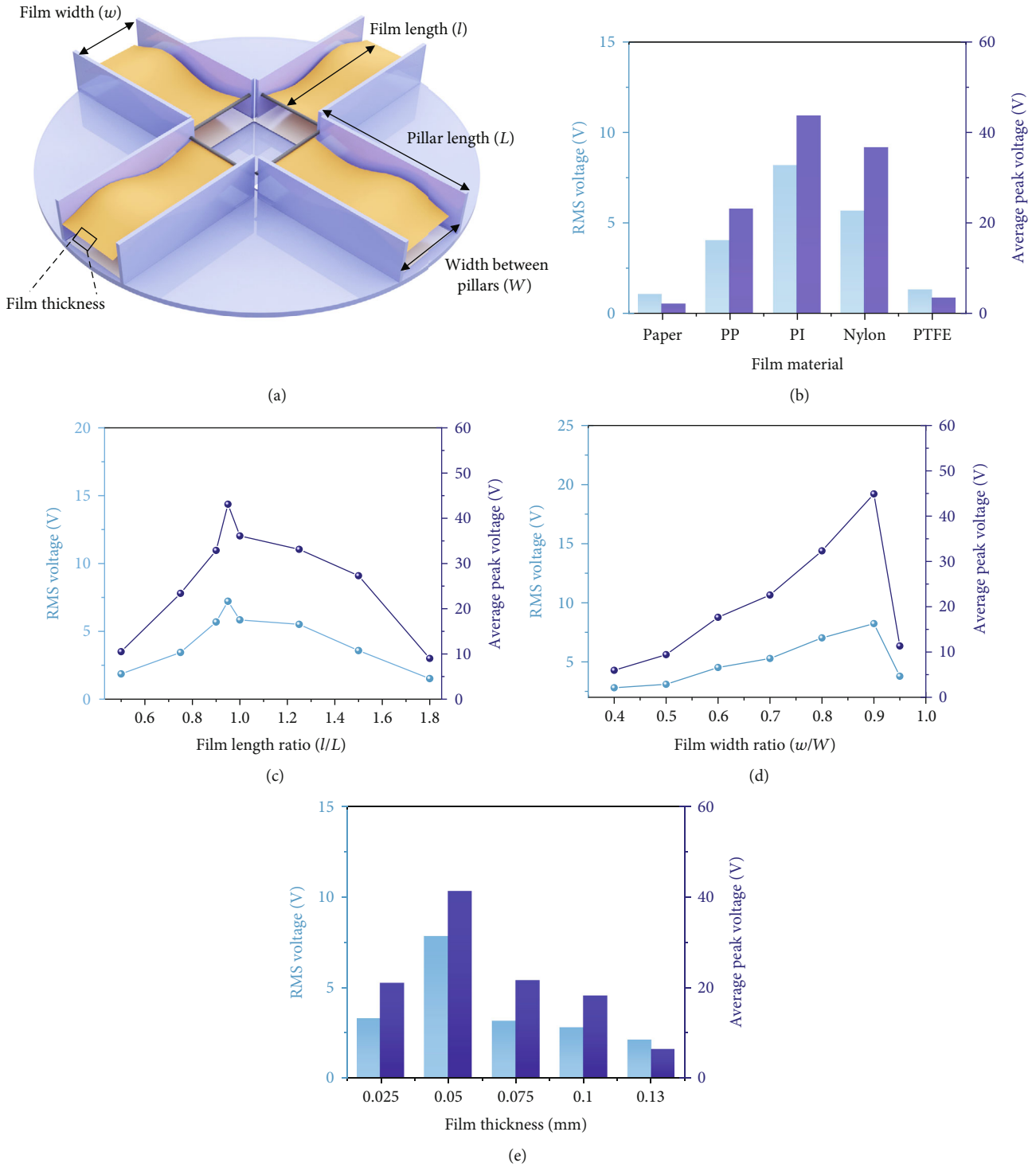

Figure 4: Optimization of fluttering TENG: (a) schematic of fluttering TENG with various design factors. RMS voltage and average peak voltage of fluttering TENG with (b) different film materials, (c) film length ratio, (d) film width ratio, and (e) film thickness.

and vertical TENG and the integration output of the fluttering and vertical TENG. This result indicates that the output of the OVFH-TENG increased when the fluttering and vertical TENG were integrated.

To determine the power increase of the OVFH-TENG compared with the general contact-separation TENG, we compared the power outputs of the OVFH-TENG and the general contact-separation TENG. The general contact-separation TENG was consisted with using PI film for the dielectric material, and the contact size was the same as OVFH-TENG. Both devices were tested with same input frequency of 4 Hz. A photograph of the general contact-

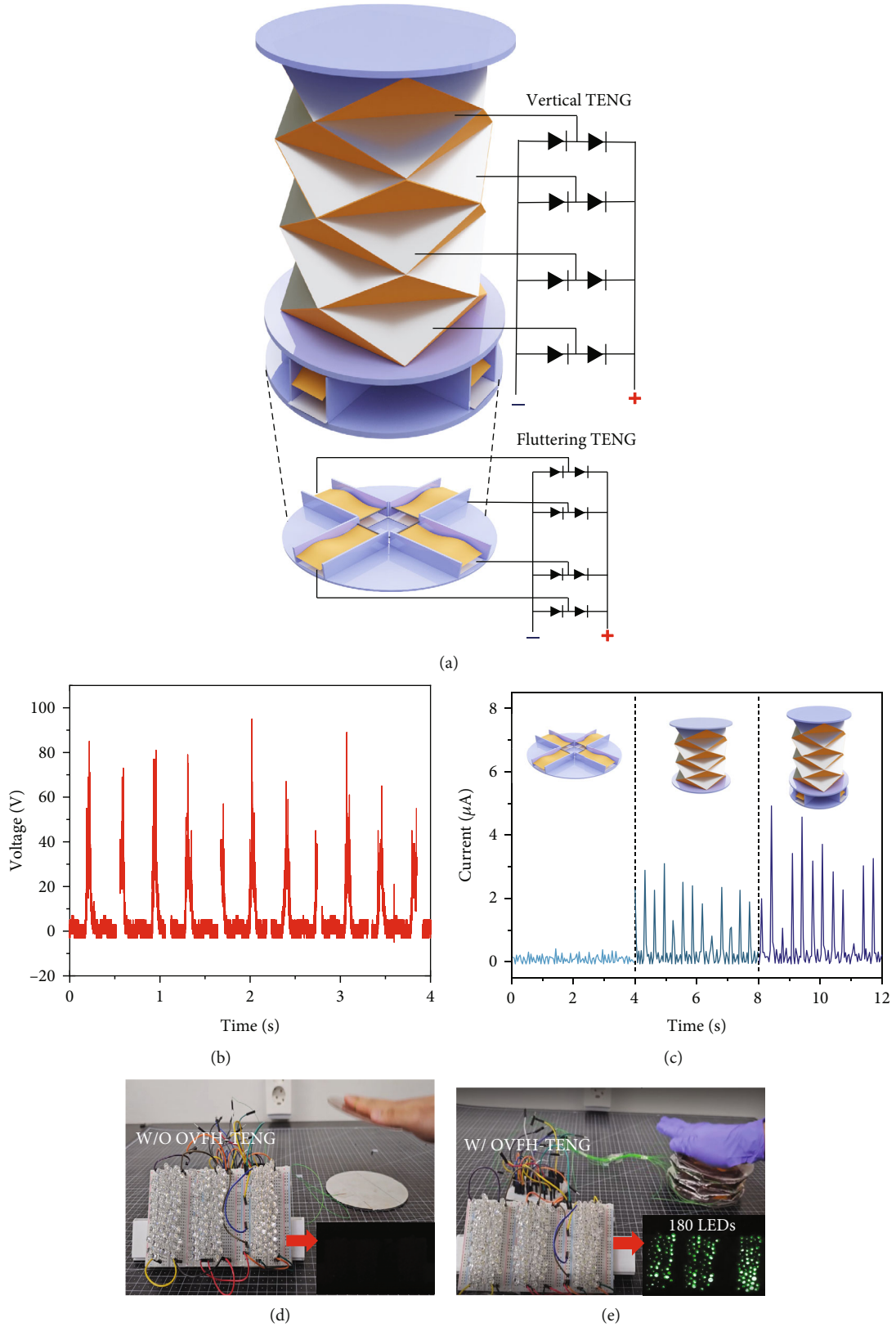

Figure 5: Integrated OVFH-TENG by vertical TENG and fluttering TENG: (a) schematic of integrated structure with rectifying circuit; (b) rectified voltage output of OVFH-TENG; (c) current output of fluttering TENG, vertical TENG, and integrated device. Photograph of LEDs by powering with (d) general contact-separation TENG and (e) OVFH-TENG.

separation TENG is shown in Figure S9. Figure S10 shows the RMS current and voltage of the general contact-separation TENG with different load resistances, and Figure S11 shows the RMS current and voltage of the HO TENG with different load resistances. Based on these results, the power outputs of the general contact-separation TENG and OVFH-TENG were calculated by multiplying the RMS current and voltage, as shown in Figure S12. Both TENGs show the highest power output with a load resistance of 10 MΩ. The general contact-separation TENG and OVFH-TENG generated 2.13 μW and 2.87 μW, respectively. This result shows that the OVFH-TENG generated 34.7% high power. In addition, because the OVFH-TENG can generate a higher output than the general TENG, the OVFH-TENG could light 180 LEDs; however, the general contact-separation TENG was unable to light 180 LEDs, as shown in Figures 5(d) and 5(e) and Video S1. Consequently, the OVFH-TENG generated a higher electrical output than the conventional contact-separation TENG. By these result, OVFH-TENG can be the potential alternative design strategy for foldable stacking TENG which can be used for harvesting vertical movement such as human movement by its own structure or rotational movement by using additional device such as crankshaft.

4. Conclusion

In this study, we fabricated an OVFH-TENG, which is a hybrid generator that integrates vertical and fluttering TENG. The OVFH-TENG can generate electrical output from both vertical contact-separation and fluttering motions using a single input owing to the Yoshimura origami pattern. To enhance the electrical output of the OVFH-TENG, the structure of the vertical TENG, such as the origami pattern and film thickness, was optimized using equations and experimental results. The structure of the fluttering TENG was optimized to generate a high electrical output. Finally, by integrating the optimized vertical TENG and fluttering TENG, the optimized OVFH-TENG generated a 34.7% higher power output than the general contact-separation TENG; therefore, the OVFH-TENG was able to light 180 LEDs that the general contact-separation TENG was unable to light. We believe that the proposed OVFH-TENG can be used as an efficient hybrid generator for harvesting mechanical energy and it can also be the potential alternative design strategy for stackable TENGs.

Data Availability

Data is available in the supplementary information files.

Conflicts of Interest

The authors declare that they have no conflicts of interest.

Authors' Contributions

Seh-Hoon Chung was responsible for the conceptualization, methodology, formal analysis, investigation, and visualization and wrote the original draft. Minsoo Kim was responsible for the conceptualization, methodology, formal analysis, investigation, and visualization and wrote the original draft. Zong-Hong Lin was responsible for the formal analysis and visualization. Bonwook Koo was responsible for the formal analysis and visualization. Dongwhi Choi was responsible for the conceptualization, methodology, supervision, and project administration. Dongseob Kim was responsible for the conceptualization, methodology, supervision, and project administration. Sangmin Lee was responsible for the conceptualization, methodology, supervision, and project administration. Seh-Hoon Chung and Minsoo Kim contributed equally to this work.

Acknowledgments

This work was supported by the National Research Foundation of Korea (NRF) grant, funded by the Korea government (MSIT) (Nos. 2022R1A2C2012254 and 2023R1A2C2006170). And we would like to thank Editage (http://www.editage.co.kr/) for English language editing.

Supplementary Materials

Supplementary information includes the detailed data. Figure S1: photograph of OVFH-TENG: (a) vertical TENG; (b) fluttering TENG. Figure S2: schematic of the wind generation that activates the fluttering TENG. Figure S3: photograph of pressed structures according to the change of θ. Figure S4: voltage outputs of vertical TENG with different numbers of attached electrodes. Figure S5: measured wind speeds generated by vertical TENG with different input frequencies. Figure S6: voltage outputs of fluttering TENG with different input frequencies. Figure S7: voltage outputs of vertical TENG before and after 80,000 cycles. Figure S8: voltage outputs of fluttering TENG before and after 80,000 cycles. Figure S9: photograph of general contact-separation TENG. Figure S10: RMS current and voltage output of general contact-separation TENG. Figure S11: RMS current and voltage output of OVFH-TENG with different load resistance. Figure S12: RMS power of general contact-separation TENG and OVFH-TENG. Video S1: 180 LEDs connected to general contact-separation TENG and OVFH-TENG. *(Supplementary Materials)*

References

[1] U. Khan and S.-W. Kim, "Triboelectric nanogenerators for blue energy harvesting," *ACS Nano*, vol. 10, no. 7, pp. 6429–6432, 2016.

[2] W.-G. Kim, D.-W. Kim, I.-W. Tcho, J.-K. Kim, M.-S. Kim, and Y.-K. Choi, "Triboelectric nanogenerator: structure, mechanism, and applications," *ACS Nano*, vol. 15, no. 1, pp. 258–287, 2021.

[3] Z. L. Wang, "Triboelectric nanogenerators as new energy technology for self-powered systems and as active mechanical and chemical sensors," *ACS Nano*, vol. 7, no. 11, pp. 9533–9557, 2013.

[4] F.-R. Fan, Z.-Q. Tian, and Z. Lin Wang, "Flexible triboelectric generator," *Nano Energy*, vol. 1, no. 2, pp. 328–334, 2012.

[5] R. Dharmasena and S. Silva, "Towards optimized triboelectric nanogenerators," *Nano Energy*, vol. 62, pp. 530–549, 2019.

[6] S.-H. Chung, Y. H. Jang, D. Kim et al., "High-output wearable flow ring-based triboelectric nanogenerator via opposite charging intermediate layer," *International Journal of Energy Research*, vol. 2023, Article ID 3415211, 8 pages, 2023.

[7] H. J. Hwang, J. S. Yeon, Y. Jung, H. S. Park, and D. Choi, "Extremely foldable and highly porous reduced graphene oxide films for shape-adaptive triboelectric nanogenerators," *Small*, vol. 17, no. 9, article e1903089, 2021.

[8] M. V. Paranjape, S. A. Graham, H. Patnam, P. Manchi, and J. S. Yu, "Multimode consecutively connected piston-type cylindrical triboelectric nanogenerators for rotational energy harvesting and sensing application," *International Journal of Energy Research*, vol. 2023, Article ID 1495217, 11 pages, 2023.

[9] Y. Zou, J. Xu, Y. Fang, X. Zhao, Y. Zhou, and J. Chen, "A hand-driven portable triboelectric nanogenerator using whirligig spinning dynamics," *Nano Energy*, vol. 83, article 105845, 2021.

[10] J. Lee, S.-H. Chung, B. Kim et al., "Wear and triboelectric performance of polymers with non-polar lubricants," *Tribology International*, vol. 178, article 108088, 2023.

[11] S. H. Chung, J. Chung, M. Song et al., "Nonpolar liquid lubricant submerged triboelectric nanogenerator for current amplification via direct electron flow," *Advanced Energy Materials*, vol. 11, no. 25, article 2100936, 2021.

[12] C. Wang, H. Guo, P. Wang, J. Li, Y. Sun, and D. Zhang, "An advanced strategy to enhance TENG output: reducing triboelectric charge decay," *Advanced Materials*, vol. 35, no. 17, article e2209895, 2023.

[13] D. Kam, G. Gwon, S. Jang et al., "Advancing energy harvesting efficiency from a single droplet: a mechanically guided 4D printed elastic hybrid droplet-based electricity generator," *Advanced Materials*, vol. 35, no. 48, article 2303681, 2023.

[14] M. M. Rastegardoost, O. A. Tafreshi, Z. Saadatnia, S. Ghaffari-Mosanenzadeh, C. B. Park, and H. E. Naguib, "Recent advances on porous materials and structures for high-performance triboelectric nanogenerators," *Nano Energy*, vol. 111, article 108365, 2023.

[15] W. Yang, X. Wang, H. Li et al., "Fundamental research on the effective contact area of micro-/nano-textured surface in triboelectric nanogenerator," *Nano Energy*, vol. 57, pp. 41–47, 2019.

[16] S.-H. Chung, K. Cha, M. Song et al., "Sub-watt power triboelectric generator via polarization switching charge carrier," *Nano Energy*, vol. 103, article 107754, 2022.

[17] S.-H. Chung, J.-h. Son, K. Cha et al., "Boosting power output of fluttering triboelectric nanogenerator based on charge excitation through multi-utilization of wind," *Nano Energy*, vol. 111, article 108389, 2023.

[18] W. Liu, Z. Wang, G. Wang et al., "Integrated charge excitation triboelectric nanogenerator," *Nature Communications*, vol. 10, no. 1, pp. 1–9, 2019.

[19] H. Zhou, X. Wei, B. Wang, E. Zhang, Z. Wu, and Z. L. Wang, "A multi-layer stacked triboelectric nanogenerator based on a rotation-to-translation mechanism for fluid energy harvesting and environmental protection," *Advanced Functional Materials*, vol. 33, no. 7, article 2210920, 2023.

[20] Y. Xie, S. Wang, S. Niu et al., "Multi-layered disk triboelectric nanogenerator for harvesting hydropower," *Nano Energy*, vol. 6, pp. 129–136, 2014.

[21] J. Cai, X. Deng, Y. Xu, and J. Feng, "Motion analysis of a foldable barrel vault based on regular and irregular Yoshimura origami," *Journal of Mechanisms and Robotics*, vol. 8, no. 2, article 021017, 2016.

[22] J.-E. Suh, T.-H. Kim, and J.-H. Han, "New approach to folding a thin-walled Yoshimura patterned cylinder," *Journal of Spacecraft and Rockets*, vol. 58, no. 2, pp. 516–530, 2021.

[23] M. Xu, Y.-C. Wang, S. L. Zhang et al., "An aeroelastic flutter based triboelectric nanogenerator as a self-powered active wind speed sensor in harsh environment," *Extreme Mechanics Letters*, vol. 15, pp. 122–129, 2017.

[24] J. H. Son, S. H. Chung, K. Cha et al., "Ultrahigh performance, serially stackable, breeze driven triboelectric generator via ambient air ionizing channel," *Advanced Materials*, vol. 35, no. 24, article 2300283, 2023.